Research Article Vol. 6, No. 7 / July 2019 / Optica 878

Nonlinear optics with full three-dimensional illumination

Rojiar Penjweini,[1,2] Markus Weber,[1,2] Markus Sondermann,[1,2,*] Robert W. Boyd,[3] and Gerd Leuchs[1,2,3]

[1]Friedrich-Alexander-Universität Erlangen-Nürnberg (FAU), Department of Physics, Staudtstr. 7/B2, 91058 Erlangen, Germany
[2]Max Planck Institute for the Science of Light, Staudtstr. 2, 91058 Erlangen, Germany
[3]Department of Physics, University of Ottawa, 25 Templeton Street, Ottawa, Ontario K1N 6N5, Canada
*Corresponding author: markus.sondermann@fau.de

Received 27 February 2019; revised 26 May 2019; accepted 11 June 2019 (Doc. ID 361161); published 11 July 2019

Nonlinear optical interactions play a crucial role in modern technology and lead to important applications such as optical switching, optical harmonic generation, and the characterization of ultrafast material processes. Nonlinear interactions are enhanced by using a tightly focused laser beam, but nonetheless they are typically excited by a loosely focused (that is, paraxial) laser beam. Here we investigate a specific process, third-harmonic generation, excited by a highly nonparaxial beam that illuminates an interaction region from a nearly full solid angle. We elucidate the influence of the focal volume and the pump intensity on the number of frequency-tripled photons by varying the solid angle from which the pump light is focused, and we find good agreement between the experiments and numerical calculations. As the pump light is focused to a spot size much smaller than the laser wavelength, the Gouy phase does not limit the yield of frequency-converted photons, in stark contrast to the paraxial regime. We believe that our findings are generic and apply to many other nonlinear optical processes when the pump light is focused from a full solid angle.

https://doi.org/10.1364/OPTICA.6.000878

1. INTRODUCTION

The first multiphoton process was described by Göppert-Mayer when calculating the spontaneous decay of the 2s state of the hydrogen atom [1]. But it took until the invention of the laser and the first investigation of second-harmonic generation by Franken and coworkers in 1961 [2] before the field of nonlinear optics took off. Since then, most of the experiments have been performed in the paraxial regime with mildly focused Gaussian beams; see Fig. 1(a). One can find only a few reports on experiments where the pump light driving the nonlinear process has been focused such that the paraxial approximation is not valid [3–7]. These investigations treated second-harmonic generation at an interface [3,4] or measured the nonlinear optical response of nanoparticles [5–7]. In a wider sense, also multiphoton-excitation microscopy [8] and stimulated-emission depletion microscopy (STED) [9] can be considered as nonlinear optics under nonparaxial conditions when using microscope objectives with a large enough numerical aperture (NA), as depicted in Fig. 1(b). There is even one report on STED in a 4Pi-microscopy setup using two microscope objectives [10], which, however, is still far away from full 4π solid angle focusing. Investigations in *isotropic* nonlinear media under clearly nonparaxial conditions are lacking.

Here, we investigate the nonlinear response under close to full-solid-angle focusing, when the transmitted beam interferes with the incoming beam to form a 4π standing wave [see Fig. 1(c)]. Such a wave is a superposition of a converging (inward propagating) and a diverging (outward propagating) dipole wave [11,12]. In this standing wave with a spherical phase front, the wave vector of the pump naturally averages to zero, while the broad spread of wave vectors has implications on the phase matching of the nonlinear optical process, as we will discuss later. This is unlike the standing wave in a cavity, where the wave vectors are typically confined within a small cone. Furthermore, the focal volume within a standing dipole wave is much smaller than a wavelength cubed [13,14]. This is a new experimental regime in which, to the best of our knowledge, no nonlinear optics experiments have been conducted so far. We perform such an experiment in studying a paradigmatic process, third-harmonic generation (THG) in an isotropic homogeneous medium (argon gas).

To focus the pump light from a full solid angle, we use a parabolic mirror (PM) with a focal length much shorter than its depth. The PM is illuminated with a radially polarized mode that after reflection off the PM's surface resembles the far-field radiation pattern of a linear electric dipole [15]. The exact expression of the spatial intensity distribution of the mode incident onto the PM is derived in Ref. [15]. In the case of a perfect PM, the mode's phase front is flat.

Upon reflection, this incident mode is transformed into a spherical standing dipole wave [11,12]. The far-field radiation pattern of a linear electric dipole is characterized by the well-known $\sin^2\vartheta$ intensity pattern, where ϑ is the polar angle of a

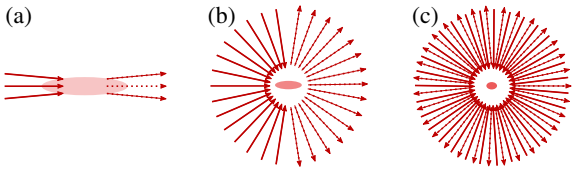

Fig. 1. Illustration of different focusing regimes. (a) Paraxial regime using low NA; (b) nonparaxial regime of focusing with high NA; (c) focusing from a full solid angle. Solid/dotted arrows represent the propagation direction of a wave propagating toward/out of the focus. In nonparaxial regimes (b) and (c), the vector properties of the field are important. The rosé ellipse in the center indicates the size of the focal spot. Note that in (c) the spot is not spherical, which is a result of the vector properties of the light, not shown in the diagrams.

spherical coordinate system with its origin at the focus. The electric field is oriented along the unit vector in ϑ direction. The ring-shaped intensity distribution implies that along the optical axis of the PM, i.e., for $\vartheta = 0$ or π, there is no light in the far-field region. Nevertheless, there is a dominant nonvanishing on-axis field component in the focal region. This longitudinally polarized component corresponds to the main near-field contribution of linear-dipole radiation and drops from its maximum value towards zero on a length scale of a wavelength.

Under such conditions, several questions as posed below arise. In order to address these questions, we briefly recall some essential features of THG with Gaussian beams in the paraxial regime (see, e.g., Ref. [16]): When the nonlinear medium is longer than twice the Rayleigh length of the Gaussian beam and the beam waist is located in the middle of the medium, the nonlinear polarization induced in the interaction region before the beam waist is 180° out of phase with the one generated in the diverging beam behind the beam waist due to the Gouy phase. Under conditions of nominal phase matching, this results in destructive interference of the light fields generated in these two distinct half-spaces. One can only compensate for the Gouy phase when choosing a nonlinear medium with a positive phase mismatch. Hence, in normally dispersive media such as noble gases driven far from resonance, where the phase mismatch is always negative, THG by four-wave mixing (FWM), i.e., the process $\omega + \omega + \omega \rightarrow 3\omega$, is not expected to occur (see, e.g., Section 2.10.3 in Ref. [16]). Thus, the generation of frequency-tripled photons can occur only as the result of higher-order processes, and accordingly, the observed power dependence is not of the third order (see, e.g., Refs. [17–24]).

When focusing from a full solid angle with a dipole-like radiation pattern, the full width at half-maximum of the spatial intensity distribution in the focus is on the order of the wavelength of the pump light or smaller. Consequently, the field amplitude of the pump light varies from practically zero to its maximum value within a wavelength and strictly violates the slowly varying amplitude approximation that is inherent to the paraxial approximation. Phase matching in the paraxial regime is equivalent to velocity matching such that the phase relation between pump, signal, and idler is preserved. In the regime with light propagating in all directions, this concept no longer makes sense. It will even turn out that over the relevant length scale of the focal pump field distribution, the phase of the pump varies so weakly that it practically can be neglected.

Therefore, one can ask the general questions: "What determines the efficiency of the nonlinear coupling in this extreme case?" "Which predictions of the paraxial approximation are still valid in the regime of extreme focusing?" "If one observes THG under this experimental condition, how will the third-harmonic signal scale with pump power and with the solid angle used for focusing?"

In this paper, we give answers to these questions. In Section 2 we describe our experimental apparatus and present the experimental results. As we will show, one indeed observes the generation of frequency-tripled photons when focusing from a large fraction of the full solid angle. Based on our observations, we identify six-wave mixing (SWM) as the underlying process, somewhat resembling other experiments in the paraxial regime [18,23,24]. Guided by this finding, we compare our experimental observations to numerical simulations. In the last section, we discuss our results and draw some further conclusions.

Beyond providing a novel scenario for nonlinear optics, a setup based on a PM spanning a full solid angle could prove to be advantageous for applications. Such a PM offers a high collection efficiency for photons emerging from the focal region [25], which is important for maximizing the yield of actually usable photons. Furthermore, a PM is essentially an achromatic device since the focusing of light (or its collimation, respectively) is based on reflection. This way the dispersion of the mirror's material has a minimized impact. This is especially important in wave-mixing processes involving different wavelengths with a large spectral separation or when the pump light itself, such as light from a frequency comb, has a broad spectrum. Last but not least, focusing a dipole wave from a full solid angle minimizes the power necessary to obtain a given field strength. This relaxes the high power requirements for sources of pump light driving the nonlinear process.

2. EXPERIMENT

A. Experimental Setup

Figure 2 shows a simplified scheme of our experimental setup. A pulsed Nd:YAG laser is used as the light source for the fundamental beam. This laser has a wavelength of 1064 nm, a pulse duration of 2 ns, a repetition rate of 50 Hz, and a pulse energy of up to 1 mJ. The beam power is adjusted by means of a half-wave plate and a polarizing beam splitter. The pump beam is transformed to a radially polarized doughnut beam by passing the fundamental Gaussian beam through a liquid-crystal polarization converter (ARCoptix, RADPOL). Unwanted modes present in the beam leaving the polarization converter are rejected by means of a spatial filter. Figure 2(b) shows the intensity distribution and the orientation-angle of the local polarization vector of the resulting beam, both determined by a spatially resolved measurement of the Stokes parameters [26]. Based on these measurements, we computed the overlap of the generated mode with the optimum mode for generating a linear dipole wave to be in excess of 90%, using the method explained in Ref. [27].

The pump beam is aligned to the PM by using two mirrors such that the beam propagates along the optical axis of the PM. The PM is made of aluminum and manufactured by single-point precision diamond-turning (Kugler GmbH, Germany). The focal length is $f = 2.1$ mm, and the diameter of the PM's exit pupil is 20 mm. In addition, the PM exhibits a bore hole of 1.5 mm diameter at its vertex. The PM is placed inside a vacuum chamber that is first evacuated to the order of 10^{-2} mbar and then filled with argon gas. The PM exhibits deviations from a perfect parabolic

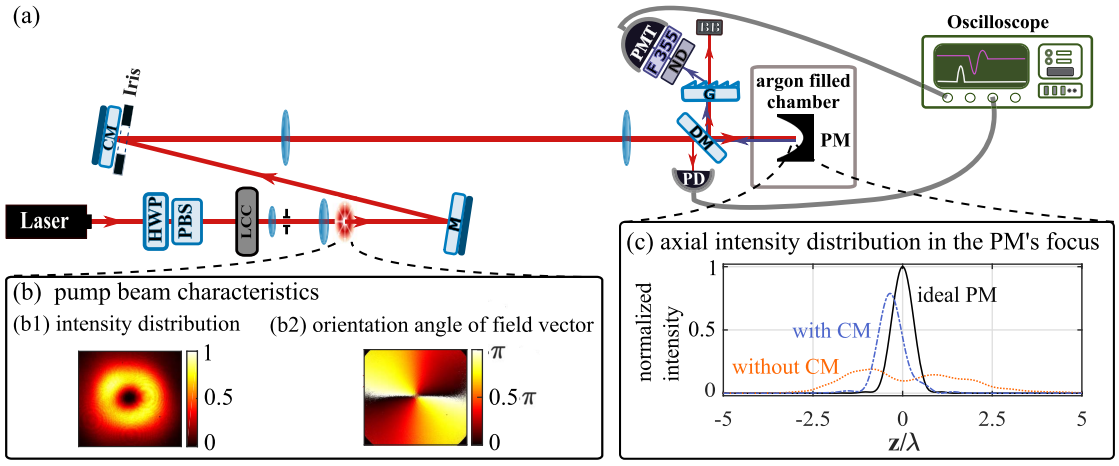

Fig. 2. (a) Scheme of the experimental setup. HWP, half-wave plate; PBS, polarizing beam splitter; LCC, liquid-crystal polarization converter; M, mirror; CM, compensation mirror; DM, dichroic mirror; PD, photodiode; PM, parabolic mirror; G, grating; BB, beam block; ND, neutral density filter; F 355, 355 nm laser-line filter; PMT, photomultiplier tube. (b) Normalized intensity distribution (b1) and spatially resolved orientation angle ψ of the polarization vector (b2) of the pump beam. $\psi = 0$ is pointing parallel to the optical table and perpendicular to the optical axis of the PM. (c) Simulated axial intensity distribution in the focal region of an aberration-free PM (black solid curve), the PM used in the experiments (orange dotted curve), and for this PM when the aberrations are partially corrected by use of the CM (blue dashed-dotted curve).

shape, introducing significant aberrations. The aberrations are characterized by interferometric measurements [28]. Based on the results of these measurements, a compensation mirror (CM) was manufactured that nominally imprints a wavefront modulation onto the incident beam that is conjugate to the one imprinted by the aberrations of the PM. The actual wavefront imprinted by the CM is also determined by interferometry. The CM serves as one of the alignment mirrors mentioned above [see Fig. 2(a)]. In order to avoid changes to the imprinted wavefront occurring upon propagation, the electric field distribution emerging from the CM is imaged 1:1 onto the entrance aperture of the PM by means of a telescope.

We have assessed the impact of the PM's aberrations and the degree of aberration compensation by the CM by simulating the focal intensity distribution for various cases exploiting all available interferometric data; see Fig. 2(c). In comparison to an aberration-free mirror, the PM alone exhibits a Strehl ratio of only 19%, i.e., the maximum intensity in the focal region is about 5 times below that observed for diffraction-limited focusing. However, the simulations predict that by using the CM, the Strehl ratio can be improved to 79%. This imperfect compensation is due to the fact that the CM does not apply the targeted phase distribution exactly.

In the experiments presented below, we investigate the generation of third-harmonic photons using different solid angles for focusing. This variation is achieved by aperturing the pump beam with an iris of adjustable size. The iris is positioned close to the CM and is thus likewise imaged onto the PM aperture with the same telescope that is used for imaging the CM. By using the relation $\tan \vartheta/2 = r/2f$ [15], one can compute the effective half-opening angle ϑ for a given iris radius r. The resulting ϑ is then used for calculating the solid angle used for focusing.

Because a strongly focused, radially polarized doughnut beam produces an electric field distribution that closely resembles that of a linear dipole oscillating along the optical axis of the focusing device [29], here we define the solid angle as the one obtained when weighted with the angular intensity emission pattern of a linear dipole: $\Omega = 2\pi \int_{\vartheta_{\min}}^{\vartheta_{\max}} \sin^2 \vartheta \cdot \sin \vartheta \mathrm{d}\vartheta$. Using this definition, Ω has an upper limit of $\frac{8\pi}{3}$ when $\vartheta_{\min} = 0$ and $\vartheta_{\max} = \pi$ [30]. The specific geometry of our PM corresponds to $\vartheta_{\min} = 20°$ and $\vartheta_{\max} \cong 134°$. Therefore, the maximum weighted solid angle covered by our PM is $0.94 \times \frac{8\pi}{3}$.

Frequency-tripled photons generated in the focal region are collimated by the PM and afterwards reflected by a dichroic mirror (DM). The same DM directs a small fraction of the incident pump pulses onto a photodiode (PD). The PD signal serves as a trigger for detecting the frequency-tripled beam. To suppress any remaining pump light in the detection path for the frequency-tripled photons, a grating (G) separates this light from the frequency-tripled beam. The pump beam is finally dumped at a beam block (BB). The frequency-tripled beam is detected by a photomultiplier tube (PMT) (Hamamatsu R11540) after passing through a 355 nm laser line filter and neutral density (ND) filters. The PMT cannot distinguish between pulses with different photon numbers. It rather responds nonlinearly to pulses with more than one photon. Therefore, the ND filters are chosen such that they attenuate the frequency-tripled beam to an average photon number per pulse smaller than unity. In all experiments, the detected average photon number per pulse is obtained from a series of about 2500–3000 laser pulses focused by the PM. Accounting for the attenuation factors of the ND filters used and other optical losses (in total 0.17%), we finally calculate the average number of frequency-tripled photons generated in the focal region of the PM.

B. Experimental Results

At first, we check whether the generation of frequency-tripled photons under strongly nonparaxial conditions is observed at all. We monitor the number of photons detected at a wavelength of 355 nm while varying the diameter of the iris limiting the beam size from 7–20 mm. These diameters correspond to solid angles $36\% \leq \Omega/(8\pi/3) \leq 94\%$. The smallest solid angle investigated here corresponds to a half-opening angle of 80° or an NA of 0.98,

respectively. Hence, all measurements are carried out under strong nonparaxial conditions. For each iris diameter, the laser power is adjusted such that the power transmitted through the iris is the same.

As is evident from Fig. 3, we indeed observe the generation of frequency-tripled photons. Upon increasing the solid angle used for focusing, one observes a higher yield of frequency-tripled photons. The number of frequency-tripled photons per pulse is affected by an interplay between the focal intensity and the focal volume as the main nonlinear interaction region, as discussed below. To investigate the generation of frequency-tripled photons in more detail and to unveil the mechanism of the frequency conversion, we measure the number of generated photons as a function of the peak power of the fundamental beam. Figure 4 shows the results for two cases of focusing from 55% and from 94% of the full solid angle. A linear fit to the data in a double-logarithmic representation produces a line with a slope of approximately 5 in both cases. Thus, the number of the generated frequency-tripled photons scales with the fifth power of the optical power of the fundamental beam.

This result answers one of the questions posed above: Under strongly nonparaxial conditions, frequency-tripled photons are not generated by a simple FWM process. In the paraxial regime, dependences of the frequency-tripled photon number on the pump power with orders ranging from 3.5–5 have been

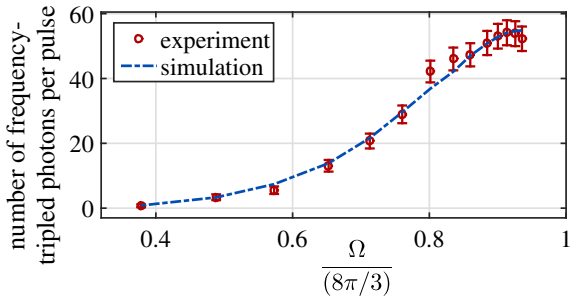

Fig. 3. Number of generated frequency-tripled photons versus the solid angle subtended by the pump beam. Red points show the experimental results for a pressure of 668 mbar and a fixed pump pulse energy of 114 μJ. The dashed-dotted blue line shows the result of a simulation when using the nonlinear susceptibility $\chi^{(5)}$ as a fit parameter (see Section 2 of Supplement 1 for simulation details).

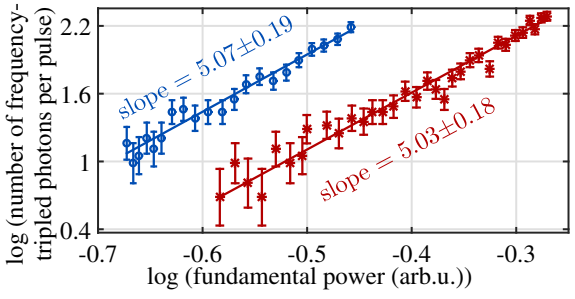

Fig. 4. Frequency-tripled photon generation versus power of the fundamental beam at a pressure of 657 mbar for two different solid angles: 55% (red stars) and 94% (blue circles) of full solid angle. The data are presented in double logarithmic scale (symbols). The error bars are obtained from the Poisson statistics of the detected photons. Lines denote the results of fitting a linear function to the respective data.

reported [17–24]. Possible explanations for this fifth-order dependence include a SWM process [18,23,24] and FWM with phase matching achieved by the Kerr effect [17,20,22]. However, our investigations exclude THG by FWM with phase matching enabled by the Kerr effect. As explained in detail in Section 1 of Supplement 1, this conclusion results from the fact that for argon gas and the pump beam powers used in our experiment, a positive phase mismatch cannot be achieved via the Kerr effect.

Therefore, as done elsewhere for several experiments in the paraxial regime [18,23,24], we attribute the generation of frequency-tripled photons in our experiments to SWM: The argon atoms absorb four photons at frequency ω and emit two photons, one of them with frequency ω and the other one with frequency 3ω. Unlike for THG with focused light, frequency-tripled generation through SWM is possible for both positive and negative phase mismatch [31]. In either case, in SWM one can compensate for the phase mismatch by suitable off-axis wave vectors (see also Ref. [23]). When focusing from large fractions of the solid angle, a broad spread of such wave vectors is readily provided. Expanding a linear-dipole wave in terms of plane waves, the probability to have a wave vector oriented under an angle ϑ to the optical axis is proportional to $\sin^2\vartheta$.

Having identified the dependence of the THG on pump power, we now discuss the dependence of THG on the solid angle in more detail: The intensity in the focus of the PM is proportional to the solid angle Ω [30]. Therefore, for a SWM process as found here one would expect the TH signal to scale with Ω^5. However, the experimental data underlying Fig. 3 reveal a slightly weaker dependence (Ω^4).

Building upon these arguments, we simulate frequency-tripled photon generation, modeling the response of the medium with a fifth-order susceptibility. The details of our theoretical simulation are explained in Section 2 of Supplement 1. In Fig. 3, we directly compare the simulation results to the experimental data. To within the experimental uncertainties, we find a good qualitative agreement between simulation and experiment. Furthermore, numerical calculations of the focal intensity distribution (shown in Fig. S3 of Supplement 1) reveal that with increasing solid angle, both the focal volume as well as the effective volume in which SWM occurs decrease approximately as $1/\Omega$. Since the distribution of the phase of the focal electric field is rather flat (see Fig. 5 and discussion below), one can approximate the number of generated photons to scale as (maximum intensity)^5 × effective volume. This results in an Ω^4 scaling, which is in good agreement with the experiment.

By fitting the simulation results to the experiment, we obtain $\chi^{(5)} = 1.53^{+0.21}_{-0.18} \times 10^{-48}$ $(\mathrm{m/V})^4/\mathrm{bar}$ as the only fit parameter. This value is of the same order of magnitude as the value reported for the case of fifth-harmonic generation in Ref. [32] and

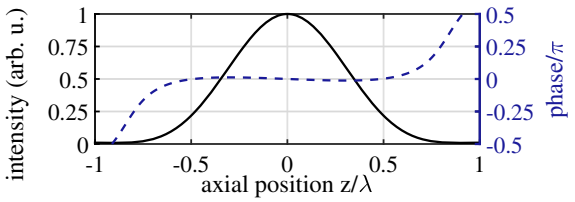

Fig. 5. Theoretical on-axis intensity (solid line) and phase distribution (dashed line) of the pump light on the optical axis of the PM when focusing with the complete PM covering 94% of the full solid angle without any aberrations.

therefore appears to be reasonable. The main uncertainty of the fitting procedure is given by the accuracy of the pump power measurements, which is about 5%. Furthermore, in implementing our model numerically, we made several approximations; see Section 3 of Supplement 1, which might influence the uncertainty of the value obtained for $\chi^{(5)}$. Nevertheless, we conclude that our model yields a good agreement with the experimental results.

3. DISCUSSION AND CONCLUSIONS

In the introduction to this paper, we raised several questions on potential differences between harmonic generation in the paraxial regime and when focusing the pump light from a full solid angle.

Indeed, also in the latter case one observes the generation of frequency-tripled photons in an isotropic medium with normal dispersion. As in the paraxial regime, one does not observe a third-order dependence of the frequency-converted photons on pump power, as expected for a FWM process. Rather, we have found a fifth-order dependence, which hints at SWM as the underlying process.

What is the origin of the suppression of the FWM contribution to THG when focusing from a full solid angle? The tempting answer might be that the Gouy phase has the same detrimental effects as in the paraxial regime. And indeed, the standing spherical waves that are generated by focusing from a full solid angle exhibit the Gouy phase, i.e., a phase shift relative to a running spherical wave that emerges from the focus [33]. But being defined in such a way, the Gouy phase does not reflect the total phase at a certain position in the focal region. As our simulations reveal, the spatial variation of the phase of the pump field in the relevant focal region is not strong enough to result in a complete suppression of an FWM signal. As shown in Fig. 5, the intensity distribution of the pump light decays more quickly towards zero than the phase of the pump field changes by $\pi/2$. This is clearly different from what is found for a focused Gaussian beam in the paraxial regime, for which a phase distribution as the one displayed in Fig. 5 can only be found when choosing an unphysical beam waist. The latter would correspond to a lateral width at half-maximum that is smaller than the minimal one obtainable in free space [14].

Another possible reason for the suppression of FWM is found when discussing wave vector diagrams (e.g., Refs. [16,23]): For an FWM process in a medium with normal dispersion, there is no combination of three wave vectors of the fundamental beam that results in a wave vector of the TH light. The wave vector mismatch is smallest for collinear wave vectors. In the experiment performed here, the strong focusing of the fundamental beam induces a large spread of the directions of the corresponding wave vectors. This large spread results in larger wave vector mismatches than in the paraxial regime. Hence the FWM process is suppressed even more strongly. Contrarily, for the SWM process, focusing from a full solid angle provides many possible combinations in which five wave vectors of the fundamental beam can be matched to a wave vector of the TH light. We thus conclude that SWM is the lowest-order process that can generate frequency-tripled photons in the case of very tight focusing.

Although we investigated the influence of full-solid-angle focusing on a specific nonlinear optical process, our findings—especially the ones about the role of the Gouy phase—are valid for all nonlinear optical processes, in particular for those of higher order. Furthermore, collecting the generated photons over a full solid angle minimizes losses and facilitates the investigation of the spatial properties of many phenomena in nonlinear optics.

Funding. Natural Sciences and Engineering Research Council of Canada (NSERC); Canada Research Chairs; Seventh Framework Programme (FP7) of the European Research Council (ERC) (Advanced Grant 'PACART').

Acknowledgment. The authors thank K. Mantel for the characterization of the CM and M. Bader for discussions.

See Supplement 1 for supporting content.

REFERENCES

1. M. Göppert-Mayer, "Über elementarakte mit zwei quantensprüngen," Ann. Phys. **401**, 273–294 (1931).
2. P. A. Franken, A. E. Hill, C. W. Peters, and G. Weinreich, "Generation of optical harmonics," Phys. Rev. Lett. **7**, 118–119 (1961).
3. E. Yew and C. Sheppard, "Second harmonic generation polarization microscopy with tightly focused linearly and radially polarized beams," Opt. Commun. **275**, 453–457 (2007).
4. D. P. Biss and T. G. Brown, "Polarization-vortex-driven second-harmonic generation," Opt. Lett. **28**, 923–925 (2003).
5. P. Reichenbach, A. Horneber, D. A. Gollmer, A. Hille, J. Mihaljevic, C. Schäfer, D. P. Kern, A. J. Meixner, D. Zhang, M. Fleischer, and L. M. Eng, "Nonlinear optical point light sources through field enhancement at metallic nanocones," Opt. Express **22**, 15484–15501 (2014).
6. A. Horneber, K. Braun, J. Rogalski, P. Leiderer, A. J. Meixner, and D. Zhang, "Nonlinear optical imaging of single plasmonic nanoparticles with 30 nm resolution," Phys. Chem. Chem. Phys. **17**, 21288–21293 (2015).
7. X. Wang, X. Zhuang, F. Wackenhut, Y. Li, A. Pan, and A. J. Meixner, "Power-and polarization dependence of two photon luminescence of single CdSe nanowires with tightly focused cylindrical vector beams of ultrashort laser pulses," Laser Photon. Rev. **10**, 835–842 (2016).
8. W. R. Zipfel, R. M. Williams, and W. W. Webb, "Nonlinear magic: multiphoton microscopy in the biosciences," Nat. Biotechnol. **21**, 1369–1377 (2003).
9. V. Westphal and S. W. Hell, "Nanoscale resolution in the focal plane of an optical microscope," Phys. Rev. Lett. **94**, 143903 (2005).
10. M. Dyba and S. W. Hell, "Focal spots of size λ/23 open up far-field florescence microscopy at 33 nm axial resolution," Phys. Rev. Lett. **88**, 163901 (2002).
11. I. M. Basset, "Limit to concentration by focusing," J. Mod. Opt. **33**, 279–286 (1986).
12. C. Cohen-Tannoudji, J. Dupont-Roc, and G. Grynberg, *Photons and Atoms* (Wiley, 1989).
13. N. Bokor and N. Davidson, "4π focusing with single paraboloid mirror," Opt. Commun. **281**, 5499–5503 (2008).
14. I. Gonoskov, A. Aiello, S. Heugel, and G. Leuchs, "Dipole pulse theory: maximizing the field amplitude from 4π focused laser pulses," Phys. Rev. A **86**, 053836 (2012).
15. N. Lindlein, R. Maiwald, H. Konermann, M. Sondermann, U. Peschel, and G. Leuchs, "A new 4π -geometry optimized for focusing onto an atom with a dipole-like radiation pattern," Laser Phys. **17**, 927–934 (2007).
16. R. W. Boyd, *Nonlinear Optics*, 3rd ed. (Academic, 2008).
17. R. A. Ganeev, M. Suzuki, M. Baba, H. Kuroda, and I. A. Kulagin, "Third-harmonic generation in air by use of femtosecond radiation in tight-focusing conditions," Appl. Opt. **45**, 748–755 (2006).
18. R. Ganeev, S. R. Kamalov, M. Kodirov, M. Malikov, A. Ryasnyansky, R. Tugushev, S. U. Umidullaev, and T. Usmanov, "Harmonic generation in organic dye vapors," Opt. Commun. **184**, 305–308 (2000).
19. G. Marcus, A. Zigler, and Z. Henis, "Third-harmonic generation at atmospheric pressure in methane by use of intense femtosecond pulses in the tight-focusing limit," J. Opt. Soc. Am. B **16**, 792–800 (1999).
20. M. S. Malcuit, R. W. Boyd, W. V. Davis, and K. Rzążewski, "Anomalies in optical harmonic generation using high-intensity laser radiation," Phys. Rev. A **41**, 3822–3825 (1990).

21. A. L'Huillier, L. Lompre, M. Ferray, X. Li, G. Mainfray, and C. Manus, "Third-harmonic generation in xenon in a pulsed jet and a gas cell," Europhys. Lett. **5**, 601 (1988).
22. R. Ganeev, V. Gorbushin, I. Kulagin, and T. Usmanov, "Optical harmonic generation in media with positive dispersion," Appl. Phys. B **41**, 69–71 (1986).
23. V. Vaičaitis, V. Jarutis, and D. Pentaris, "Conical third-harmonic generation in normally dispersive media," Phys. Rev. Lett. **103**, 103901 (2009).
24. V. Vaičaitis, V. Jarutis, K. Steponkevičius, and A. Stabinis, "Noncollinear six-wave mixing of femtosecond laser pulses in air," Phys. Rev. A **87**, 063825 (2013).
25. R. Maiwald, A. Golla, M. Fischer, M. Bader, S. Heugel, B. Chalopin, M. Sondermann, and G. Leuchs, "Collecting more than half the fluorescence photons from a single ion," Phys. Rev. A **86**, 043431 (2012).
26. B. Schaefer, E. Collett, R. Smyth, D. Barrett, and B. Fraher, "Measuring the Stokes polarization parameters," Am. J. Phys. **75**, 163–168 (2007).
27. A. Golla, B. Chalopin, M. Bader, I. Harder, K. Mantel, R. Maiwald, N. Lindlein, M. Sondermann, and G. Leuchs, "Generation of a wave packet tailored to efficient free space excitation of a single atom," Eur. Phys. J. D **66**, 190 (2012).
28. G. Leuchs, K. Mantel, A. Berger, H. Konermann, M. Sondermann, U. Peschel, N. Lindlein, and J. Schwider, "Interferometric null test of a deep parabolic reflector generating a Hertzian dipole field," Appl. Opt. **47**, 5570–5584 (2008).
29. S. Quabis, R. Dorn, M. Eberler, O. Glöckl, and G. Leuchs, "Focusing light to a tighter spot," Opt. Commun. **179**, 1–7 (2000).
30. M. Sondermann, N. Lindlein, and G. Leuchs, "Maximizing the electric field strength in the foci of high numerical aperture optics," arXiv:0811.2098 (2008).
31. J. Kutzner and H. Zacharias, "VUV generation by frequency tripling the third harmonic of a picosecond kHz Nd:YLF laser in xenon and mercury vapour," Appl. Phys. B **66**, 571–577 (1998).
32. X. F. Li, A. L'Huillier, M. Ferray, L. A. Lompré, and G. Mainfray, "Multiple-harmonic generation in rare gases at high laser intensity," Phys. Rev. A **39**, 5751–5761 (1989).
33. T. Tyc, "Gouy phase for full-aperture spherical and cylindrical waves," Opt. Lett. **37**, 924–926 (2012).